Interacting Multiple Model Filter-Based Sensor Fusion of GPS With In-Vehicle Sensors for Real-Time Vehicle Positioning

Kichun Jo, *Student Member, IEEE*, Keounyup Chu, *Student Member, IEEE*, and Myoungho Sunwoo, *Member, IEEE*

***Abstract*—Vehicle position estimation for intelligent vehicles requires not only highly accurate position information but reliable and continuous information provision as well. A low-cost Global Positioning System (GPS) receiver has widely been used for conventional automotive applications, but it does not guarantee accuracy, reliability, or continuity of position data when GPS errors occur. To mitigate GPS errors, numerous Bayesian filters based on sensor fusion algorithms have been studied. The estimation performance of Bayesian filters primarily relies on the choice of process model. For this reason, the change in vehicle dynamics with driving conditions should be addressed in the process model of the Bayesian filters. This paper presents a positioning algorithm based on an interacting multiple model (IMM) filter that integrates low-cost GPS and in-vehicle sensors to adapt the vehicle model to various driving conditions. The model set of the IMM filter is composed of a kinematic vehicle model and a dynamic vehicle model. The algorithm developed in this paper is verified via intensive simulation and evaluated through experimentation with a real-time embedded system. Experimental results show that the performance of the positioning system is accurate and reliable under a wide range of driving conditions.**

***Index Terms*—Information fusion, interacting multiple mode (IMM) filter, in-vehicle sensors, vehicle positioning.**

I. Introduction

THE IMPORTANCE of accuracy and integrity in a positioning system has increasingly been emphasized for intelligent transportation system (ITS) applications based on position information, including advanced driver-assistance systems, electronic toll collection, intersection collision warnings, and traffic control. Today, the satellite-based Global Positioning System (GPS) is widely used for such applications because the GPS receiver provides vehicle position and velocity data in global coordinates. However, a standalone GPS receiver cannot fulfill the positioning requirements of ITS applications due to the occasional temporary loss of satellite connection and signal errors. To provide continuous, accurate, and high integrity position data, the positioning system should be aided by additional sensors such as an inertial navigation system (INS), vehicle motion sensors, digital road maps, cameras, radar, or laser scanners [1].

The fusion of GPS data with data from INS is a common solution for positioning systems due to the complementary natures of these two types of sensors [1]–[9]. However, the installation of an INS requires extra cost and effort, and accurate INS systems are too expensive for automotive applications. On the other hand, passenger cars equipped with a vehicle stability control system already utilize vehicle motion sensors such as wheel speed sensors, a yaw rate sensor, an accelerometer, and a steering sensor [10]–[12]. In addition, the accuracy and reliability of these in-vehicle sensors are increasingly being developed for multiple safety and comfort applications [13], [14]. Therefore, the fusion of data from in-vehicle sensors with GPS data becomes sufficiently accurate and reliable for the vehicle positioning system without additional cost or sensor installation. Information regarding the external vehicle environment from vision sensors, radar, and laser scanners can also be used with the data from the positioning system by integrating the information into a digital map that has highly accurate road features [15]–[27].

Numerous Bayesian filter-based sensor fusion approaches have been proposed for use with the positioning algorithm [28]. The extended Kalman filter (EKF) is the most widely used for information fusion algorithms because nonlinear localization problems can easily be solved using this filter [10]–[12], [29]. Although the EKF provides efficient and reliable performance for practical applications, the linearization process can lead to divergence in a highly nonlinear system. To prevent this problem, advanced nonlinear filtering methods such as the particle filter were introduced [30]. However, this method requires excessive computational power to be implemented in embedded systems.

The performance of a positioning system depends not only on the filter structure but also on the appropriate choice of process model for the Bayesian filter. The roles of the process models in positioning systems were investigated in [31], which demonstrated significantly better performance for a positioning algorithm that had a good process model compared with that of

Manuscript received October 13, 2010; revised June 29, 2011 and September 16, 2011; accepted September 18, 2011. Date of publication December 6, 2011; date of current version March 5, 2012. This work was supported in part by the National Research Foundation of Korea funded by the Korean government under Grant 2011-0017495, by the Ministry of Knowledge Economy, by the Korea Institute for Advancement in Technology through the Workforce Development Program in Strategic Technology, by the Ministry of Education, Science, and Technology through the BK21 Program under Grant 201000000000173, and by the Industrial Strategy Technology Development Program of the Ministry of Knowledge Economy under Grant 10039673. The Associate Editor for this paper was M. Da Lio.

K. Jo and K. Chu are with the Automotive Control and Electronics Laboratory (ACE Lab), Department of Automotive Engineering, Hanyang University, Seoul 133-791, Korea (e-mail: jokihaha@hanyang.ac.kr; acehev@hanyang.ac.kr).

M. Sunwoo is with the Department of Automotive Engineering, Hanyang University, Seoul 133-791, Korea (e-mail: msunwoo@hanyang.ac.kr).

Color versions of one or more of the figures in this paper are available online at http://ieeexplore.ieee.org.

Digital Object Identifier 10.1109/TITS.2011.2171033

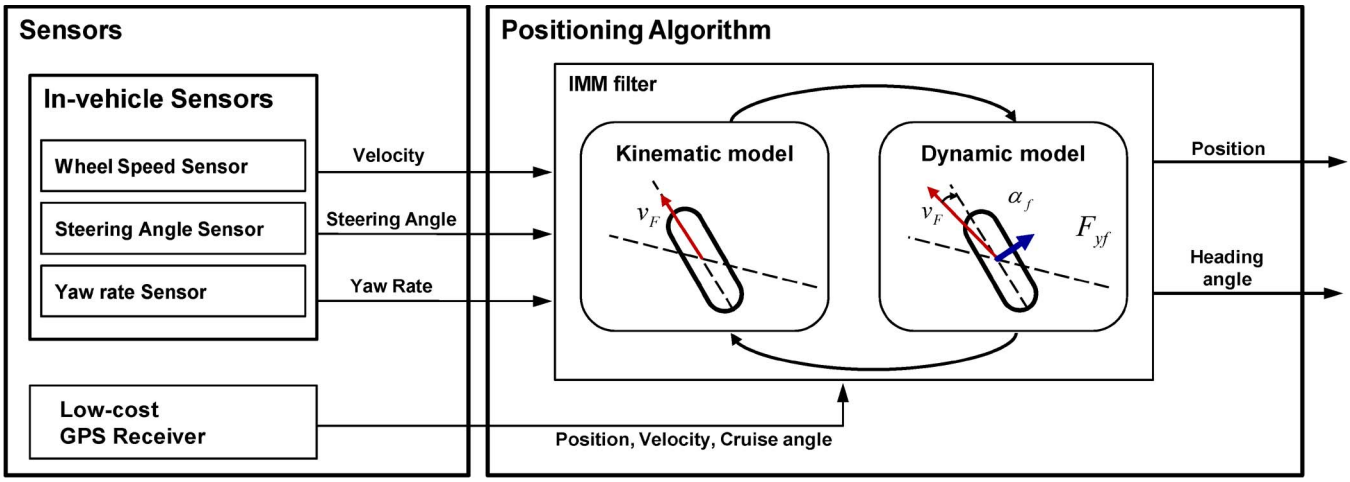

Fig. 1. Overall architecture of the IMM-based positioning system.

an algorithm with a poor process model, despite the use of the same sensor suites and number of states in all algorithms.

The major problem is that it is very difficult to choose an optimal model for all driving conditions. Higher-order advanced vehicle models that can account for various driving conditions are not suitable for positioning systems because of the unobservability of some of the parameters and the heavy computing load in real-time embedded systems. To adapt the vehicle model for application under variable driving conditions, an innovation-based adaptive estimation technique such as an input estimation method and a variable state dimension approach is proposed [32]. However, this method is complicated and inefficient.

As an alternative, the multiple model (MM) approach was proposed. This approach assumes that the system follows one of a finite number of different models. The possible vehicle driving patterns are represented by a set of models, and vehicle state information is obtained by combining specific model filters. Among several MM estimate methods, the interacting MM (IMM) estimator is the most popular due to its high performance and low computational power [32]–[34]. Therefore, the IMM filter has been used for localization and tracking problems in several studies [5], [8], [35]–[37]. In those studies, the MM filters contributed to adapt the different maneuvering states. The MM set that consists of maneuvering and nonmaneuvering states originated from the object target tracking applications that cannot directly inform the target maneuvering information [34], [38]. However, the information of maneuvering conditions of ego-vehicle can be obtained immediately from steering sensors and wheel speed sensors. In the ego-vehicle positioning, the estimation of vehicle motion aided by in-vehicle sensors will improve the performance of positioning [39]. Therefore, in this paper, dynamic vehicle characteristics such as lateral force and tire slip angle are integrated into the MM set.

This paper presents an IMM filter-based positioning algorithm that considers the variety of driving conditions in which a vehicle can be operated. To adapt to changing vehicle dynamic characteristics under various driving conditions, the MM set of the IMM filter includes both kinematic and dynamic vehicle models. While the kinematic vehicle model is appropriate for low speeds and small wheel slip driving conditions such as those in an intersection or parking lot, the dynamic vehicle model is suitable for high speeds and large wheel slip conditions, such as experienced in normal traffic and highway conditions. The IMM filter weights the appropriate vehicle model according to the driving conditions using a stochastic process. Therefore, the IMM filter-based positioning system is able to provide better accurate positional information than can single model filter-based positioning algorithms under various driving conditions.

The rest of this paper is organized as follows. Section II discusses the overall system architecture. Next, the system model set is defined in Section III. In Section IV, the IMM filter is described. The simulation and experimental results are presented in Sections V and VI, respectively, and conclusions are offered in the final section.

II. System Architecture

Fig. 1 describes the overall architecture of the proposed positioning system that is classified into a sensor part and a positioning algorithm part. The sensor part is composed of a group of in-vehicle sensors and a low-cost GPS receiver. Currently, many passenger cars are equipped with a vehicle stability control system and a GPS-based in-car navigation system. The essential components of the vehicle stability control system include several vehicle motion sensors, such as a yaw rate sensor, an accelerometer, wheel speed sensors, and a steering angle sensor. The vehicle motion data from the sensors can easily be obtained from in-vehicle sensor networks, such as the controller area network (CAN). Therefore, the positioning algorithm that estimates the vehicle position by combining the vehicle motion data with GPS can immediately be implemented in such passenger vehicles.

A low-cost GPS receiver that has widely been used for in-car navigation applications allows for the determination of global positioning and velocity estimates of a vehicle with a bounded error. However, although a GPS can provide absolute positional information, the measurement frequency is low and discontinuous. Furthermore, signals from a GPS are affected by

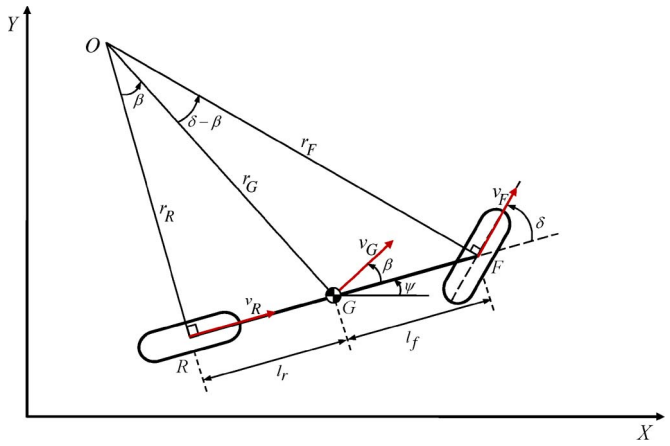

Fig. 2. Kinematic vehicle model. This model assumes no tire slip between the wheels and the ground.

the external environment. In contrast, vehicle motion sensors provide continuous measurements and are not affected by the external environment; however, they are prone to integral errors due to sensor drift. The complementary features of the two types of sensors permit the positioning systems to achieve increased update rates, accuracy, and integrity due to application of the information fusion algorithm.

In the positioning algorithm, the IMM filter-based information fusion algorithm calculates the position and heading angle estimates by combining the data from GPS and in-vehicle motion sensors. The vehicle model set of the IMM filter is composed of a kinematic vehicle model and a dynamic vehicle model. The kinematic vehicle model is based on the assumption of no wheel slip. This model is suitable for low-speed and low-slip driving conditions, such as those in an intersection or a parking lot, because the process noise of the lateral force of the vehicle does not affect the filter estimation process. However, under high-speed and large wheel slip driving conditions, the assumptions of the kinematic vehicle model break down, resulting in poor estimation performance. Therefore, the dynamic vehicle model, which considers lateral tire force and vehicle moments, can be applied to these types of situations. By combining estimates from individual model-based EKFs using the interacting process of the IMM filter, the positioning system improves the accuracies of positional and heading angle information over a wide range of driving conditions.

III. Vehicle Model Set

The performance of the IMM-based positioning algorithm depends on the design and selection of the model set. For superior performance, the model set should be able to represent a wide range of vehicle motion patterns. In this paper, the kinematic and dynamic vehicle models are used to represent possible types of vehicle motion.

A. Kinematic Vehicle Model

The kinematic vehicle model was derived from the kinematic relationships in a fundamental bicycle model, as shown in Fig. 2 [40]. In the bicycle model, the pairs of left and right wheels of a vehicle are represented by single wheels. The front steering angle is described by δ, and the center of gravity CG of the vehicle is at point G. The distances from the CG to the front and rear wheels are represented by l_f and l_r, respectively. In addition, (X, Y) represents the location of the CG in the global frame, ψ describes the heading angle of the vehicle, and v_G represents the velocity at the CG, which produces a vehicle slip angle β.

The kinematic vehicle model assumes that there is no tire slip between the wheels and the ground; therefore, the velocity vectors v_F and v_R at points F and R are in the direction of the orientation of the front and rear wheels, respectively. This assumption is reasonable for low-speed motion of the vehicle. At low speeds, the lateral force that is generated by the tires can be represented by the following centrifugal force equation:

$$F_y = \frac{m v_G^2}{r_G} \tag{1}$$

which varies with the quadratic of vehicle speed v_G. At low-speed driving conditions, since the lateral forces are very small and negligible, the velocity vectors at each wheel are almost the same as the direction of the tire.

The point O is the instantaneous rotation center for the vehicle and is defined by the intersection of lines OF and OR, which are perpendicular to the orientation of the front and rear wheels, respectively. The radius of the vehicle path r_G can be obtained from the length of the line OG that connects the center of gravity G to the instantaneous rotation center O. The velocity at G is perpendicular to the line OG, and the direction of the velocity at G with respect to the longitudinal axis of the vehicle is represented by the vehicle slip angle β. The angle ψ is defined as the heading angle of the vehicle, and the term $\psi + \beta$ is the course angle of the vehicle.

By applying the sine rule to triangles OGF and OGR, the following equations can be obtained:

$$\frac{\sin(\delta - \beta)}{l_f} = \frac{\sin\left(\frac{\pi}{2} - \delta\right)}{r_G} \tag{2}$$

$$\frac{\sin\beta}{l_r} = \frac{\sin\left(\frac{\pi}{2}\right)}{r_G}. \tag{3}$$

By rearranging (2) and (3)

$$\frac{\sin\delta\cos\beta - \sin\beta\cos\delta}{l_f} = \frac{\cos\delta}{r_G}$$

$$= \tan\delta\cos\beta - \sin\beta = \frac{l_f}{r_G} \tag{4}$$

$$\sin\beta = \frac{l_r}{r_G}. \tag{5}$$

Adding (4) and (5)

$$\tan\delta\cos\beta = \frac{l_f + l_r}{r_G}. \tag{6}$$

If we assume that the radius of the vehicle path r_G slowly changes due to the low vehicle speed, then the rate of change of

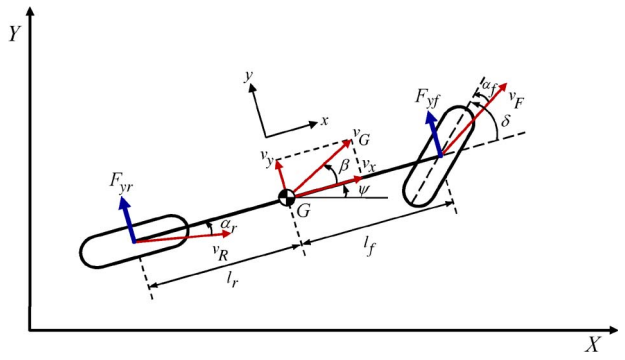

Fig. 3. Dynamic vehicle model. This model assumes that the lateral force acting on a tire is proportional to the tire slip angle.

orientation of the vehicle should be equal to the angular velocity of the vehicle γ as follows:

$$\gamma = \dot{\psi} = \frac{v_G}{r_G}. \tag{7}$$

Using (7), (6) can be rewritten as

$$\dot{\psi} = \frac{v_G}{l_f + l_r} \cos(\beta) \tan(\delta). \tag{8}$$

The vehicle slip angle β can be calculated by subtracting (4) from (5) as

$$\beta = \tan^{-1}\left(\frac{l_r \tan\delta}{l_f + l_r}\right). \tag{9}$$

The global motion of the vehicle can be defined from the course angle $\psi + \beta$ and the vehicle velocity v_G as

$$\begin{aligned} \dot{X} &= v_G \cos(\psi + \beta) \\ \dot{Y} &= v_G \sin(\psi + \beta). \end{aligned} \tag{10}$$

B. Dynamic Vehicle Model

The kinematic vehicle model is reasonable for low-speed vehicle motion because the lateral force generated by the tires is very small. In contrast, at higher speeds or with sharp steering, the no-wheel-slip assumption breaks down due to the lateral force. In this situation, the dynamic vehicle model should be considered to determine the lateral velocity of the vehicle.

To account for vehicle slip and lateral velocity, we used a dynamic vehicle model for lateral vehicle motion, as shown in Fig. 3 [41], [42]. The following equation describes the lateral dynamics of the bicycle model and was derived by summing the forces and moments about the center of gravity, where m and I_z describe the vehicle mass and the yaw moment of inertia, whereas γ, v_x, and v_y represent the yaw rate and vehicle longitudinal and lateral velocities, respectively [40]:

$$\begin{aligned} \sum F_y &= F_{yf} + F_{yr} = ma_y = m(\dot{v}_y + v_x\gamma) \\ \sum M_z &= l_f F_{yf} - l_r F_{yr} = I_z \ddot{\psi}. \end{aligned} \tag{11}$$

The dynamic vehicle model assumes that the lateral force acting on a tire is proportional to the tire slip angle, as represented in (12). The tire slip angle can be defined as the angle of the wheel velocity vector relative to the longitudinal wheel axis, i.e.,

$$\begin{aligned} F_{yf} &= 2C_f\alpha_f \approx 2C_f\left(\beta + \frac{l_f\dot{\psi}}{v_x} - \delta\right) \\ F_{yr} &= 2C_r\alpha_r \approx 2C_r\left(\beta - \frac{l_r\dot{\psi}}{v_x}\right) \end{aligned} \tag{12}$$

where C_f and C_r represent the front and rear tire cornering stiffness, and the tire slip angles of the front and rear wheels are represented by α_f and α_r, respectively.

We can calculate the overall vehicle motion of the dynamic vehicle model using the following equation:

$$\begin{aligned} \dot{\beta} &= -\gamma + \frac{2C_f}{mv_x}\left(\delta - \beta - \frac{l_f\gamma}{v_x}\right) + \frac{2C_r}{mv_x}\left(-\beta + \frac{l_r\gamma}{v_x}\right) \\ \dot{\gamma} &= \frac{2\,C_f\,l_f}{I_z}\left(\delta - \beta - \frac{l_f\gamma}{v_x}\right) - \frac{2\,C_r\,l_r}{I_z}\left(-\beta + \frac{l_r\gamma}{v_x}\right) \\ \dot{\psi} &= \gamma \\ \dot{X} &= v_G\cos(\psi + \beta) \\ \dot{Y} &= v_G\sin(\psi + \beta). \end{aligned} \tag{13}$$

IV. Interrupting Multiple Model Filter Structure

The proposed IMM-based positioning system calculates the model probabilities and integrates the EKF estimates of each model using a stochastic process to adapt to a wide range of driving conditions. Under high-speed and high-slip driving conditions, the dynamic vehicle model-based filter is more appropriate because it considers the lateral force and slip of a vehicle. In contrast, under low-speed and low-slip driving conditions, the kinematic vehicle model-based filter provides better positioning performance because the slip angle of the tire is sufficiently small to satisfy the kinematic model assumption. In addition, since the lateral force of the vehicle is very small, it can cause a numerical divergence problem for the dynamic vehicle model EKF.

The overall process of the IMM filter for the proposed positioning system is shown in Fig. 4. Using the stochastic processes, the IMM filter weighs a suitable vehicle model for the external driving conditions and estimates the position and heading angle. The IMM filter is composed of four parts: interacting, filtering, model probability updating, and estimation fusion.

A. Interacting

Initially, the states from the previous step of each model are combined with the mixing weight in the IMM filter. The mixing weight can be written as

$$\mu^{j|i}_{k-1|k-1} = \frac{1}{\hat{\mu}^i_{k|k-1}}\pi_{ji}\mu^j_{k-1}, \quad i,\ j = 1, 2 \tag{14}$$

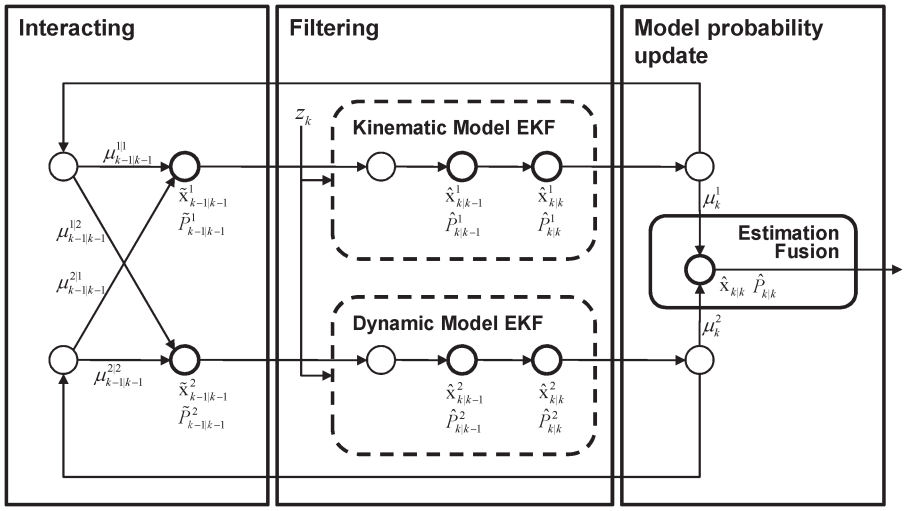

Fig. 4. Process of the IMM filter.

where μ_{k-1}^{j} is the model probability of model j in the previous step, and π_{ji} is the probability of a transition from model j to model i. The mixing probabilities $\hat{\mu}_{k|k-1}^{i}$ are described as

$$\hat{\mu}_{k|k-1}^{i} = \sum_{j=1}^{2} \pi_{ji}\mu_{k-1}^{j} \quad i = 1, 2. \tag{15}$$

The model transition of the IMM filter is governed by a first-order Markov assumption that the current state variables contain all the information needed to characterize the probability distribution for the next time step. The model transition probability matrix π_{ji} describes the probability that the vehicle model will make a transition from model state j to i. These probabilities are assumed to be *a priori* known parameters and can be represented as a probability transition matrix

$$\pi_{ji} = \begin{bmatrix} 0.9803 & 0.0197 \\ 0.0066 & 0.9934 \end{bmatrix} \tag{16}$$

where the index number i, $j = 1$ represents the kinematic vehicle model, and the index number i, $j = 2$ refers to the dynamic vehicle model. These values were calculated using a statistical method related to the sojourn times and sampling interval of the real traffic condition [8], [43].

The initial mixing state $\tilde{x}_{k-1|k-1}^{i}$ and the initial mixing covariance $\tilde{P}_{k-1|k-1}^{i}$ of model i are

$$\tilde{x}_{k-1|k-1}^{i} = \sum_{j=1}^{2} \hat{x}_{k-1|k-1}^{j}\mu_{k-1|k-1}^{j|i} \quad i = 1, 2 \tag{17}$$

$$\begin{aligned} \tilde{P}_{k-1|k-1}^{i} = & \sum_{j=1}^{2} \mu_{k-1|k-1}^{j|i} \\ & \times \left[\hat{P}_{k-1|k-1}^{j} + \left(\hat{x}_{k-1|k-1}^{j} - \tilde{x}_{k-1|k-1}^{i} \right) \right. \\ & \left. \times \left(\hat{x}_{k-1|k-1}^{j} - \tilde{x}_{k-1|k-1}^{i} \right)^{T} \right] \\ & i = 1, 2 \end{aligned} \tag{18}$$

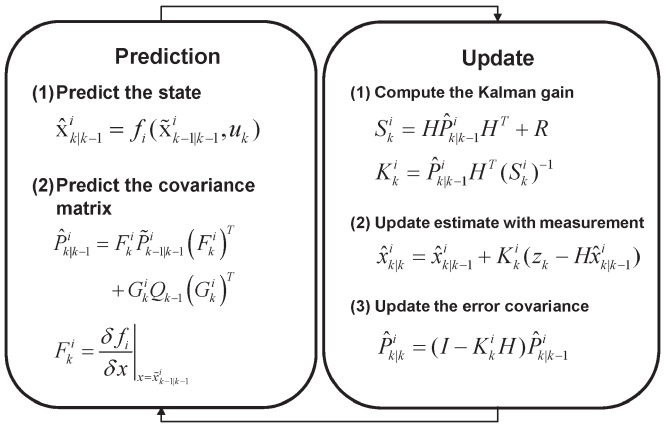

Fig. 5. EKF for each single model filter.

where $\hat{x}_{k-1|k-1}^{j}$ and $\hat{P}_{k-1|k-1}^{j}$ are the state and covariance of model j in the previous step, respectively.

B. Model-Matched Filtering

Using the initial mixing state and the covariance of the interacting step, the EKF of each model predicts and updates the model state and covariance. The overall operation of the discrete EKF for model i is shown in Fig. 5 [44].

1) Prediction With the Process Model: In the prediction step, the predicted state $\hat{x}_{k|k-1}^{i}$ and its covariance $\hat{P}_{k|k-1}^{i}$ are calculated. To obtain the predicted state and covariance at time step k, the continuous process models for the kinematic model (8)–(10) and the dynamic model (13) should be transferred into the discrete process model for numerical evaluation and implementation of the filtering system on a digital microprocessor. To execute the process model in real time, Euler's method, which is a first-order numerical process for solving a differential equation, was used. Equation (19), shown below, represents the approximation process of Euler's method, i.e.,

$$\begin{aligned} \dot{x} &\cong \frac{x_k - x_{k-1}}{T} \\ &\Rightarrow x_k \cong x_{k-1} + \dot{x} \cdot T \end{aligned} \tag{19}$$

where T represents the sampling period of the filtering system. This approximation substitutes for all the derivatives that appear in the differential equation of the process model. Using Euler's approximation process, the discrete process models for the kinematic vehicle model and the dynamic vehicle model are defined as follows:

Discrete kinematic vehicle model equation:

$$x_k^1 = f_1\left(x_{k-1}^1, u_k\right) = \begin{bmatrix} v_{\text{whl}} \\ \tan^{-1}\left(l_r \tan(\delta_{SAS})/(l_f + l_r)\right) \\ v_{k-1}\cos(\beta_{k-1})\tan(\delta_{SAS})/(l_f + l_r) \\ \psi_{k-1} + T\gamma_{k-1} \\ X_{k-1} + Tv_{k-1}\cos(\psi_{k-1} + \beta_{k-1}) \\ Y_{k-1} + Tv_{k-1}\sin(\psi_{k-1} + \beta_{k-1}) \end{bmatrix}. \tag{20}$$

The discrete dynamic vehicle model equation is shown in (21) at the bottom of the page.

The states of both vehicle models are represented as

$$x_k = [v_k \quad \beta_k \quad \gamma_k \quad \psi_k \quad X_k \quad Y_k]^T \tag{22}$$

and the model input is described as

$$u_k = [v_{\text{whl}} \quad \delta_{SAS}]^T \tag{23}$$

where v_{whl} and δ_{SAS} describe the data from the wheel speed sensor and the steering angle sensor, respectively. Using these discrete process model equations, the next predicted state $\hat{x}_{k|k-1}^i$ can be calculated as

$$\hat{x}_{k|k-1}^i = f_i\left(\tilde{x}_{k-1|k-1}^i, u_k\right), \quad i = 1, 2 \tag{24}$$

where $\tilde{x}_{k-1|k-1}^i$ refers to the initial mixing state in the interacting step. The covariance of the predicted state $\hat{P}_{k|k-1}^i$ can be obtained as

$$\hat{P}_{k|k-1}^i = F_k^i \tilde{P}_{k-1|k-1}^i \left(F_k^i\right)^T + G_k^i Q_{k-1} \left(G_k^i\right)^T, \quad i = 1, 2 \tag{25}$$

where F_k^i represents the Jacobian of the nonlinear process model

$$\left.\frac{\delta f_i}{\delta x}\right|_{x=\tilde{x}_{k-1|k-1}^i} = F_k^i, \quad i = 1, 2 \tag{26}$$

G_k^i describes the gain matrix of the process noise, and Q_{k-1} is the covariance matrix of the process noise. The parameter uncertainties of the kinematic and dynamic vehicle models are assumed to be within the allowable range of the EKF process noise.

For the implementation of the EKF of the discrete dynamic vehicle model, stable conditions using Euler's method should be achieved. Although the continuous dynamic vehicle model is stable, the discretized model might numerically be unstable due to the simple approximation of Euler's method. In particular, since the dynamic model contains the inverse of vehicle speed $1/v$, the solution of the difference equation could numerically be unstable at low-speed conditions with a long sampling period. This problem can be solved with a higher order discretization method or fast sampling rate. However, these solutions are undesirable for implementation of a real-time embedded system. In contrast to the discrete dynamic vehicle model, which has the numerical problem, the numerical stability of the kinematic vehicle model is independent of the vehicle speed and sampling period.

2) Measurement Update: In the update step, the EKF updates the corrected state $\hat{x}_{k|k}^i$ and covariance $\hat{P}_{k|k}^i$ using measurement data from the yaw rate sensor and the GPS receivers. While the yaw rate sensor provides reliable vehicle yaw rate information, which is independent of the external environment, the data from the GPS receiver are affected by several external noise sources such as lack of visible satellites, change in the distribution of visible satellites, GPS signal blockage, and multipath. Therefore, variation in the noise characteristics of GPS due to the external environment should be considered when using the measurement update step of the EKF. In this paper, a rule-based update method and a validation gate are applied for the EKF to consider such noise changes.

Rule-based measurement update: If the GPS receiver was not affected by external noise, then the measurement vector can be represented as

$$z_k = [v_{\text{GPS}} \quad \gamma_{\text{yawrate}} \quad (\beta + \psi)_{\text{GPS}} \quad X_{\text{GPS}} \quad Y_{\text{GPS}}]^T \tag{27}$$

where v_{GPS} and $(\beta + \psi)_{\text{GPS}}$ describe the velocity and course angle, X_{GPS} and Y_{GPS} represent the global positions from the GPS receiver, respectively, and γ_{yawrate} is the yaw rate from the in-vehicle sensor network. The sampling rate of the in-vehicle sensor is faster than the sampling rate of the GPS receiver, and it is synchronized to the execution rate of the filtering algorithm. Therefore, the yaw rate data can always be

$$x_k^2 = f_2\left(x_{k-1}^2, u_k\right) = \begin{bmatrix} v_{\text{whl}} \\ \beta_{k-1} + T\left[-\gamma_{k-1} + \frac{2C_f}{mv_{k-1}}\left(\delta_{SAS} - \beta_{k-1} - \frac{l_f\gamma_{k-1}}{v_{k-1}}\right) + \frac{2C_r}{mv_{k-1}}\left(-\beta_{k-1} + \frac{l_r\gamma_{k-1}}{v_{k-1}}\right)\right] \\ \gamma_{k-1} + T\left[\frac{2\,C_f\,l_f}{I_z}\left(\delta_{SAS} - \beta_{k-1} - \frac{l_f\gamma_{k-1}}{v_{k-1}}\right) - \frac{2\,C_r\,l_r}{I_z}\left(-\beta_{k-1} + \frac{l_r\gamma_{k-1}}{v_{k-1}}\right)\right] \\ \psi_{k-1} + T\gamma_{k-1} \\ X_{k-1} + Tv_{k-1}\cos(\psi_{k-1} + \beta_{k-1}) \\ Y_{k-1} + Tv_{k-1}\sin(\psi_{k-1} + \beta_{k-1}) \end{bmatrix} \tag{21}$$

used for an element of the measurement vector. However, this measurement vector cannot be used for all update steps because the noise characteristics of GPS vary depending on the external driving conditions.

Since the vehicle velocity v_{GPS} and the course angle $(\beta+\psi)_{\mathrm{GPS}}$, which were obtained from the GPS receiver, are based on the Doppler effect, the noise variances of these outputs depend on the vehicle speed [45]. At low speed less than a certain threshold $V_{\min}$, the noise variance usually increases significantly. Therefore, it is reasonable to ignore the GPS velocity and course angle measurements at low speeds. The low-speed condition can be determined by the wheel speed v_{whl} from the in-vehicle sensor network, which is independent of the GPS signal conditions. The measurement vector at the low-speed condition can be represented as

$$z_k = [\gamma_{\mathrm{yawrate}} \quad X_{\mathrm{GPS}} \quad Y_{\mathrm{GPS}}]^T. \tag{28}$$

The condition of the GPS signal can be inferred by the information from the GPS receiver, including the number of satellites $numOfSat$ and the horizontal dilution of precision $hdop$. If $numOfSat$ drops below a certain threshold $N_{\min}$ or $hdop$ exceeds a threshold $H_{\max}$, then all of the data from the GPS receiver are neglected by the EKF. The thresholds $N_{\min}$ and $H_{\max}$ are obtained experimentally. In addition, because the execution rate of the filtering algorithm is usually faster than the sampling rate of the GPS receiver, the EKF cannot update the measurements of the GPS if the receiver was not sampled. At these conditions, only yaw rate data are included in the measurement vector according to

$$z_k = [\gamma_{\mathrm{yawrate}}]^T. \tag{29}$$

All of the rule-based measurement update algorithms are described in the following pseudocode:

```
01 IF gpsUpdate is true THEN
02  IF numOfSat < N_min or hdop > H_max THEN
03   z_k = [γ_yawrate]^T
04   H = [0 0 1 0 0 0]
05  ELSE IF v_whl < V_min THEN
06   z_k = [γ_yawrate X_GPS Y_GPS]^T
07   H = [0 0 1 0 0 0
          0 0 0 0 1 0
          0 0 0 0 0 1]
08  ELSE IF
09   z_k = [v_GPS γ_yawrate (β+ψ)_GPS X_GPS Y_GPS]^T
10   H = [1 0 0 0 0 0
          0 0 1 0 0 0
          0 1 0 1 0 0
          0 0 0 0 1 0
          0 0 0 0 0 1]
11  END IF
12 ELSE IF
13  z_k = [γ_yawrate]^T
14  H = [0 0 1 0 0 0]
15 END IF
```

Validation gate: A validation gate describes a threshold that is associated with the acceptability of the measurement data. The validation gate can be calculated using the measurement vector z_k, the predicted state from the prediction step $\hat{x}^i_{k|k-1}$, and the associated covariance matrix S^i_k, as represented in the following:

$$\begin{aligned}\tilde{V}^i_k(g^2) &= \left\{ z : \left[z_k - H\cdot\hat{x}^i_{k|k-1}\right]^T \left[S^i_k\right]^{-1} \right. \\ &\qquad \left. \times \left[z_k - H\cdot\hat{x}^i_{k|k-1}\right] \le g^2 \right\} \\ &= \left\{ z : \left[v^i_k\right]^T \left[S^i_k\right]^{-1} \left[v^i_k\right] \le g^2 \right\}, \quad i = 1,2 \end{aligned} \tag{30}$$

where v^i_k is the innovation, and g is the number of sigma [46]. The associated covariance matrix S^i_k can be described as

$$S^i_k = H\hat{P}^i_{k|k-1}H^T + R. \tag{31}$$

The validation gate is the ellipsoidal volume in the measurement space, and if the measurement vector lies inside the validation gate, then these values are considered to be valid measurements. If the measurement vector lies outside the validation gate due to sudden erroneous data from the GPS receiver, then the filtering algorithm discards the value in the update step.

After the measurement vector is chosen, the EKF updates the corrected state $\hat{x}^i_{k|k}$ and covariance $\hat{P}^i_{k|k}$ using the following equation:

$$\begin{aligned}\hat{x}^i_{k|k} &= \hat{x}^i_{k|k-1} + K^i_k\left(z_k - H\hat{x}^i_{k|k-1}\right) \\ \hat{P}^i_{k|k} &= \left(I - K^i_k H\right)\hat{P}^i_{k|k-1} \\ K^i_k &= \hat{P}^i_{k|k-1}H^T\left(S^i_k\right)^{-1}. \end{aligned} \tag{32}$$

C. Mode Probability Update

The likelihood function of each mode i at time k, under the Gaussian assumption, is given by

$$\Lambda^i_k = \frac{\exp\left[-\frac{1}{2}\left(\nu^i_k\right)^T\left(S^i_k\right)^{-1}\nu^i_k\right]}{\sqrt{\left|2\pi S^i_k\right|}} \tag{33}$$

where ν^i_k and S^i_k are the innovation and its covariance, respectively.

The model probability update is calculated as follows:

$$\mu^i_k = \frac{1}{c}\Lambda^i_k\bar{c}_i \tag{34}$$

where c is the normalization constant for the mode probability update

$$c = \sum_{j=1}^{2}\Lambda^j_k\bar{c}_j. \tag{35}$$

TABLE I
VEHICLE PARAMETERS

Vehicle parameter	Value	Uncertainty (1σ)	Unit
Mass m	1832.23	300	kg
Yaw moment of inertia I_z	3120	100	kgm^2
Distance from the CG to the front wheel l_f	1415	200	mm
Distance from the CG to the rear wheel l_r	1692	200	mm
Front tire cornering stiffness C_f	262180	10000	N/rad
Rear tire cornering stiffness C_r	219034	10000	N/rad

TABLE II
SENSOR PROPERTIES

Sensor	Noise (RMS)	Bias	Unit
Yaw rate sensor	0.5	0.1	deg/s
Steering angle sensor	0.2	0	deg
Wheel speed sensor	0.3	0.5	m/s
GPS position	5	0	m
GPS velocity	1	0	m/s
GPS course angle	0.5	0	deg

D. Estimation Fusion

According to the Gaussian mixture equation, the combined state $\hat{x}_{k|k}$ and its covariance $\hat{P}_{k|k}$ are calculated as

$$\hat{x}_{k|k} = \sum_{i=1}^{2} \mu_k^i \hat{x}_{k|k}^i \tag{36}$$

$$\hat{P}_{k|k} = \sum_{i=1}^{2} \mu_k^i \left[\hat{P}_{k|k}^i + \left(\hat{x}_{k|k}^i - \hat{x}_{k|k} \right) \left(\hat{x}_{k|k}^i - \hat{x}_{k|k} \right)^T \right]. \tag{37}$$

V. SIMULATION

The proposed positioning algorithm was analyzed through intensive simulation, the results of which are averages of 100 Monte Carlo simulations. The simulation was performed using Carsim, a commercial software package for the simulation of vehicle dynamics. The parameters of the simulated vehicle model are shown in Table I, and the properties of the equipment sensors are described in Table II. The uncertainty in the model parameters and the noise of each sensor was assumed to be Gaussian white noise. Positional information from a GPS receiver was emulated by summing the position data from the reference vehicle model and the assumed GPS noise, and the in-vehicle sensors were similarly emulated. The wheel speed sensor information and the steering angle sensor information were used as inputs for the process model during the EKF prediction step. The data from the yaw rate sensor and the GPS receiver were used as measurements for the update step.

A. Characteristic of the Tire Slip Angle

The tire slip characteristics were analyzed using a steady-state cornering test, performed under a constant steering angle of two degrees and several constant velocity conditions. Fig. 6 shows the tire slip angles of the four wheels and the bicycle model. The front and rear tire slip angles of the bicycle model can be obtained as the average of the right and left tire slip angles. According to Fig. 6, the faster vehicle velocity causes larger slip angles in the front and rear tires under steady-state cornering conditions.

B. Evaluation of the IMM Filter

The simulation was carried out under variable speed conditions with a constant steering angle of two degrees. Fig. 7 represents the vehicle speeds in the simulation, including the data of the emulated wheel speed sensor. To analyze the IMM filter for several tire slip conditions, the vehicle speed varied from 2.5 to 22.5 m/s. Fig. 8(a) describes the model probability that was calculated using the IMM filter, and Fig. 8(b) shows the Euclidean distance error of each single model EKF and the IMM filter. Since the lateral tire slip was very small at low-speed conditions, the kinematic vehicle model was used to represent the vehicle motion. The performances of the IMM filter and the kinematic vehicle model EKF were nearly equal, and the IMM filter had less error than did the dynamic vehicle model EKF estimate. At the high-speed condition, because the lateral tire slip affects the vehicle dynamics, the model probability of the dynamic vehicle model in the IMM filter was greater than that of the kinematic vehicle model. This result indicates that the dynamic vehicle model is more suitable for high-slip driving conditions compared with the kinematic vehicle model. In addition, the Euclidean distance error of the IMM filter was almost the same as the error of the dynamic vehicle model EKF.

VI. EXPERIMENT

The vehicle used to conduct the experiments was a small SUV equipped with a vehicle stability control system, as shown in Fig. 9. The vehicle motion data from the stability control system could be obtained from the in-vehicle network CAN.

The noise specifications of the in-vehicle sensors are represented in Table III. The low-cost GPS receiver, SiRFstar III, which combined a small ceramic patch antenna with a low-power GPS chipset, was used for the measurements of the positioning system. The update rate of the GPS receiver was 4 Hz, and the noise specifications of the GPS are described in Table IV. The IMM-based positioning algorithm was implemented in a real-time embedded system that contained a 32-bit real-time microcontroller unit (Freescale MPC5567). The sampling rate of the implemented positioning algorithm was 40 Hz. To evaluate the performance of the proposed

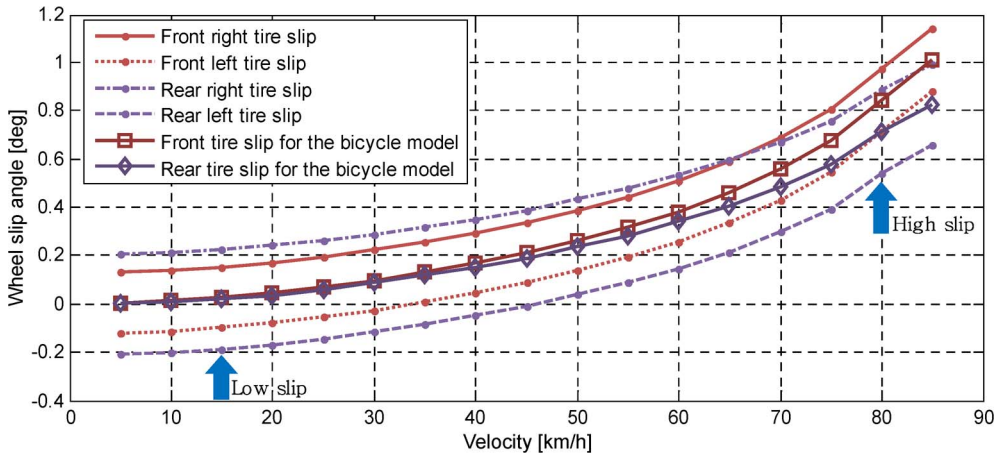

Fig. 6. Tire slip angle under a constant steering angle of two degrees and several constant speeds.

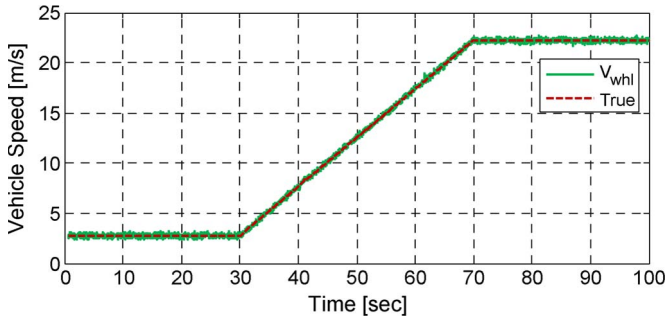

Fig. 7. Variable vehicle speed simulation. The Euclidean distance errors and the model probability for low-speed and small tire slip conditions.

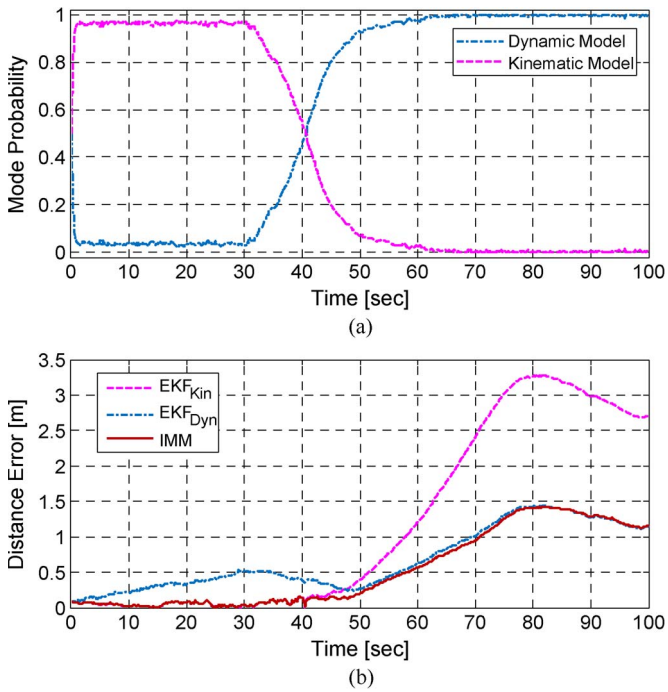

Fig. 8. Model probability and Euclidean distance errors for various speed conditions.

positioning system, an accurate localization system that integrated two differential GPSs (DGPSs) with an INS was used as a reference. In the case of DGPS blockage, the localization system was evaluated through comparison with road data from satellite maps.

The experimental evaluation was performed in two test environments. The first region included several driving conditions, such as parking lots, curved roads, and intersections. In this region, the adaptation performance of the positioning algorithm was evaluated. The second region had poor GPS conditions since this area contained many tall buildings. The continuity and reliability of the positioning system were confirmed in this region.

A. Evaluation of the Positioning Algorithm in Several Driving Environments

Fig. 10 represents a map of the test region used for the evaluation of IMM filter adaptation performance. The region included several driving environments, such as parking lots (1, 10), curved roads (2–4), and intersections (5–9). The vehicle speed and steering input are described in Fig. 11. The parking lots (1, 10) and intersections (5–9) represent the low-speed and small tire slip condition, and the curved roads (2–3) represent the high-speed and large tire slip condition.

Fig. 12 describes the model probability that was calculated using the IMM filter. The model probability represents the suitability of the vehicle model for the driving conditions. On the small slip curved road, the model probability of the kinematic vehicle model was larger than that of the dynamic vehicle model. According to this result, the kinematic vehicle model is more suitable for low-slip driving conditions than the dynamic vehicle model. In contrast, in the large-slip curved road, the model probability of the dynamic vehicle model was greater than that of the kinematic vehicle model, indicating that the dynamic vehicle model is more appropriate for high-slip regions than the kinematic vehicle model.

Fig. 13 shows the detailed logged data of the positioning system for each driving condition, where the red line represents the reference trajectory from the positioning system that combined the two DGPSs with an INS. The brown dashed-dotted line represents the filtering result of a single kinematic vehicle model EKF, and the pink dashed line represents the filtering results of a single dynamic vehicle model EKF. The

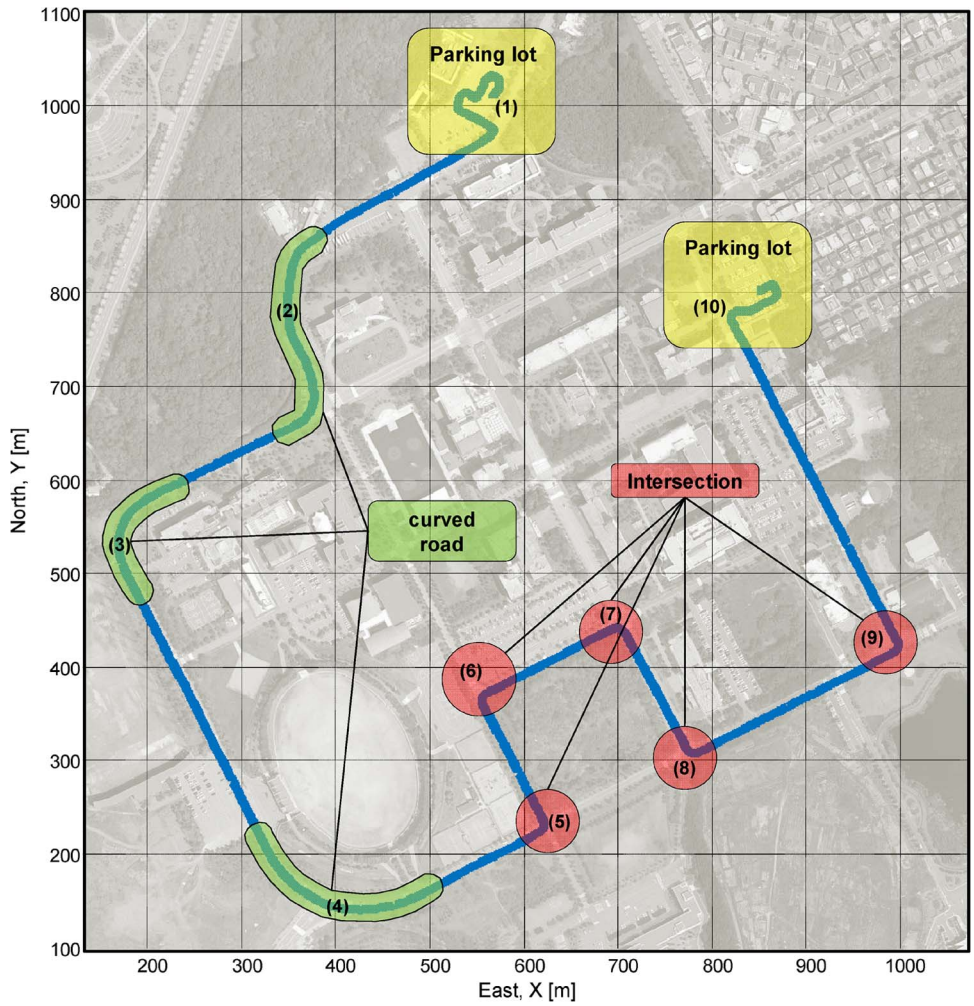

Fig. 9. Test vehicle equipped with a vehicle stability control system.

TABLE III
NOISE SPECIFICATIONS OF IN-VEHICLE SENSORS

Sensor	Range	Resolution	Noise (RMS)	Unit
Yaw rate sensor	± 120	0.0625	0.5	*deg/s*
Steering angle sensor	± 200	0.006	0.2	*deg*
Wheel speed sensor	0−130	0.035	0.3	*m/s*

TABLE IV
NOISE SPECIFICATIONS OF GPS

Sensor	Noise (CEP)	Unit
GPS	3	*m*

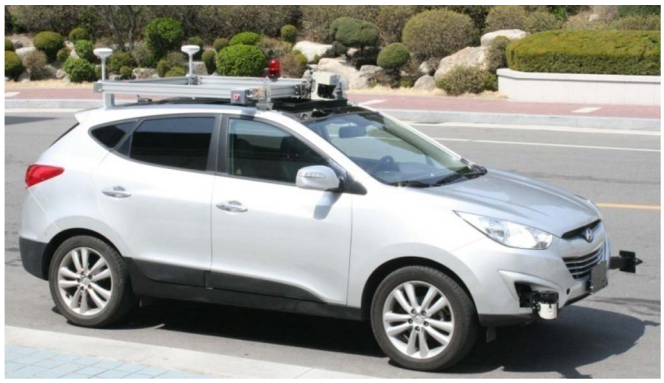

Fig. 10. Test region for the evaluation of the adaptation performance.

blue line illustrates the results of the proposed positioning system based on the IMM filter. Fig. 14 shows the Euclidean distance error of each single model EKF and the IMM filter. For the low-speed and small tire slip condition, the estimation using a dynamic vehicle model had a numerical divergence problem due to the small lateral force. Therefore, the results of the dynamic model EKF had large distance errors, as shown in Fig. 13(a) and (d). In this case, the IMM filter attributed a large amount of weight to the kinematic vehicle model for the estimation process. In contrast, for the high-speed and large tire slip region, the estimation using a kinematic vehicle model contained large distance errors due to the exclusion of the tire slip angle, as shown in Fig. 13(b) and (c). In this case, the IMM filter attributed more weight to the dynamic vehicle model compared with that of the kinematic vehicle model.

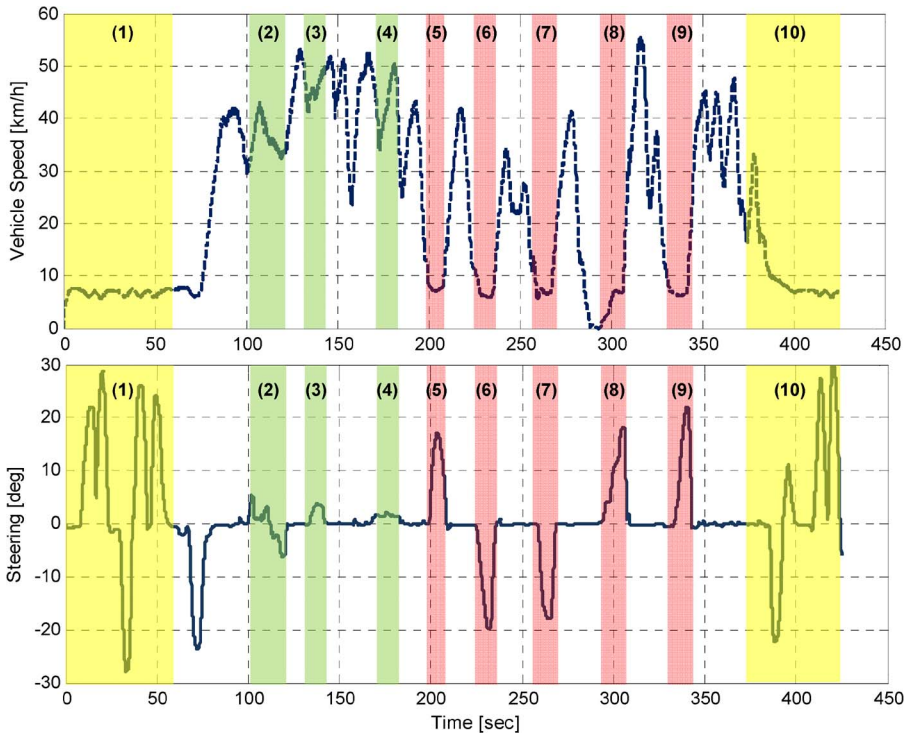

Fig. 11. Vehicle speed and steering input.

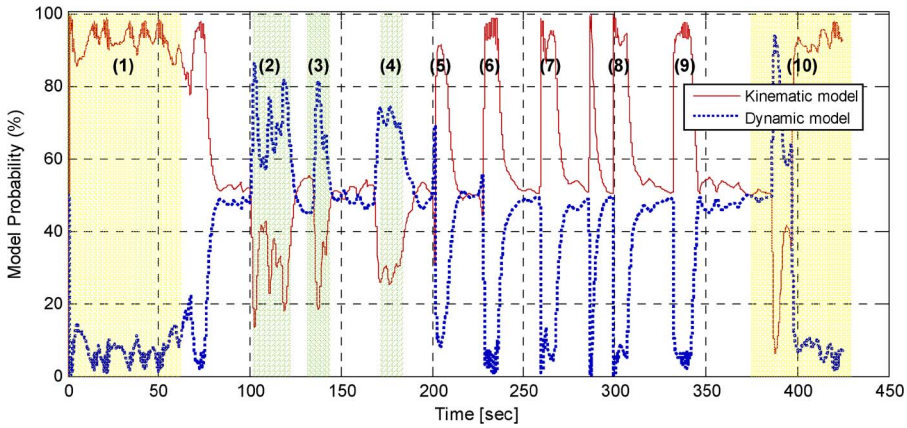

Fig. 12. Model probability of the IMM filter.

B. Bad GPS Conditions

Fig. 15 shows the map of the test region used for the evaluation of the continuity and reliability of the positioning algorithm. The green dash line represents the reference trajectory from the satellite map, the blue line represents the proposed positioning algorithm results, the red dots represent the low-cost GPS positional data, and the boxes represent tall buildings. Fig. 16 shows the number of satellites used for position estimation using the GPS and the horizontal dilution of precision (HDOP). Since the region included many tall buildings, the GPS signal was frequently blocked, as shown in regions a and b of Fig. 16.

To consider the GPS blockage and the poor GPS information, a rule-based filter update method with a validation gate was applied for the positioning algorithm. The algorithm did not update the GPS measurements when the number of satellites in used was less than or equal to four or when the HDOP was greater than five. The validation gate was installed to detect and reject drift errors due to the multipath GPS signal. Therefore, the positioning algorithm was shown to provide continuous and reliable position information even in a harsh GPS signal environment.

VII. Conclusion

In this paper, we have described the development of a vehicle positioning system that is robust to changes in driving conditions for use in ITS applications. The developed positioning algorithm integrates information from a low-cost GPS receiver with that of in-vehicle sensors. Using in-vehicle sensors and low-cost GPS, which are already installed in the vehicle stability control system, along with an in-car navigation system, the

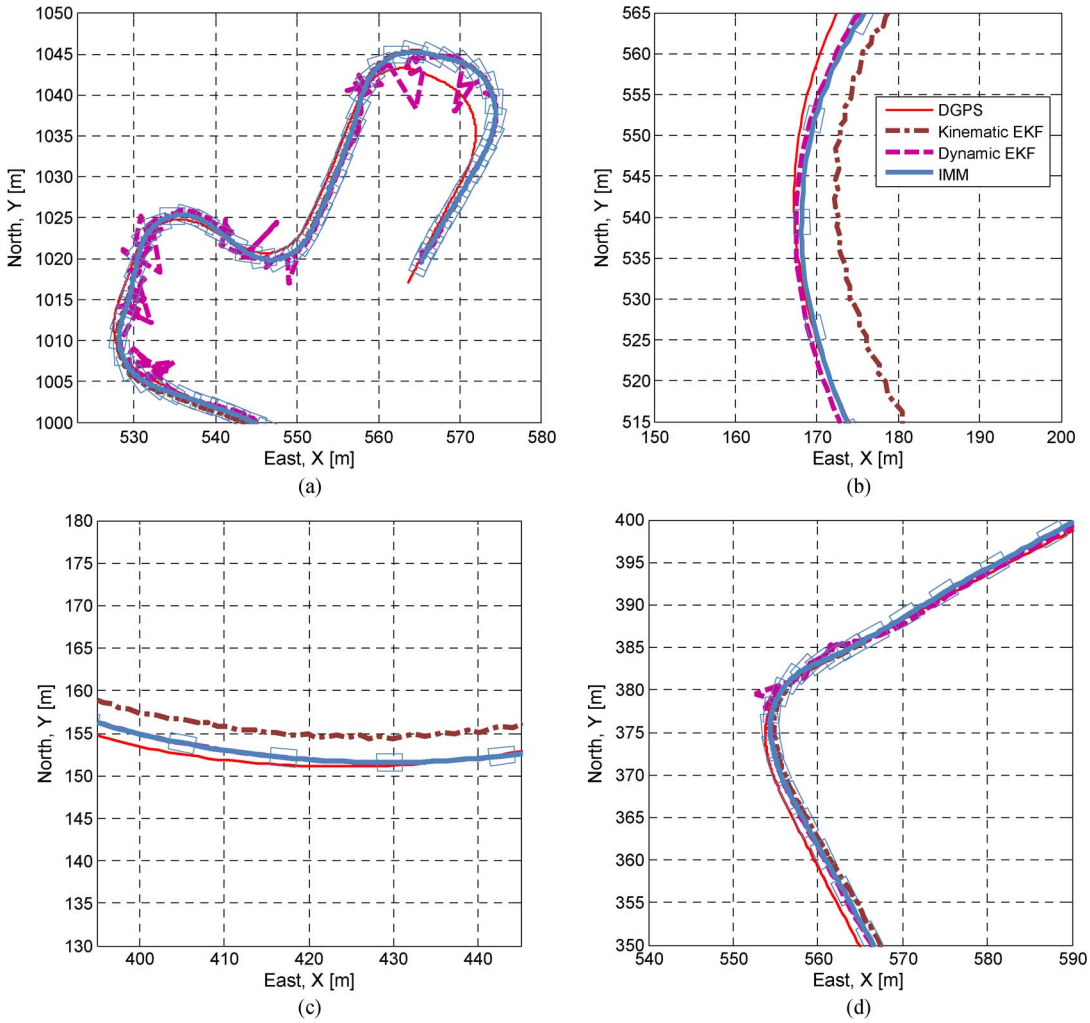

Fig. 13. Positioning system results for each driving condition.

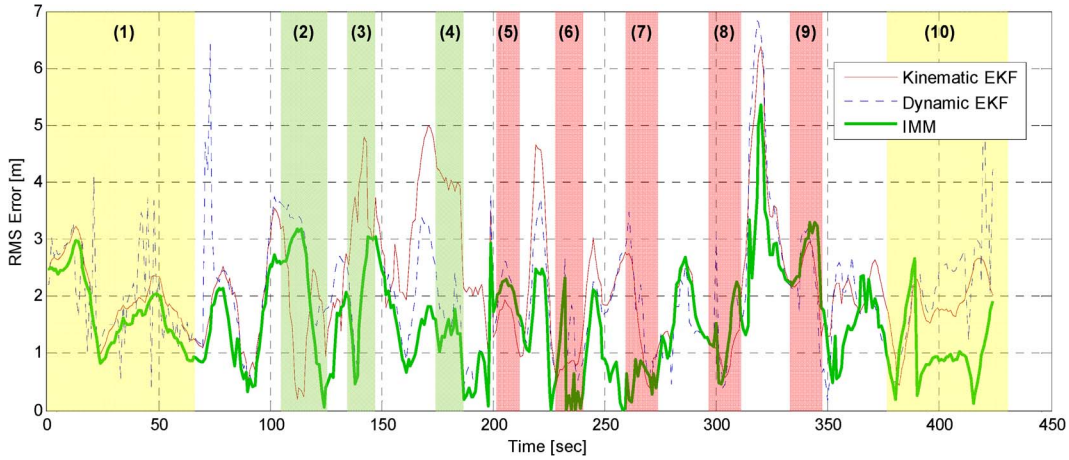

Fig. 14. Euclidean distance errors for each single model EKF and for the IMM filter.

positioning algorithm can immediately be implemented in such commercial vehicles.

The proposed IMM-based positioning system combines the EKF estimates from both kinematic and dynamic vehicle models to allow it to adapt to variable driving conditions. Under high-slip driving conditions, the estimate of the dynamic vehicle model-based filter is emphasized by the IMM filter since it considers lateral force. In contrast, for the low-speed and small tire slip condition, the estimates of the kinematic vehicle model-based filter are preferentially used for the IMM filter because the process noise of the lateral vehicle velocity does not affect the filter estimation process.

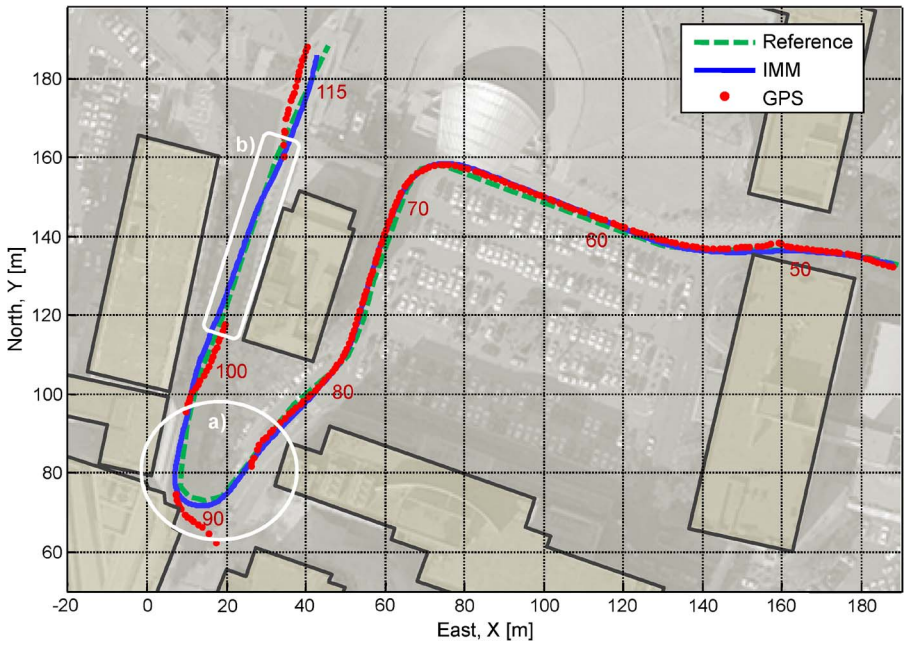

Fig. 15. Test region for evaluation of continuity and reliability.

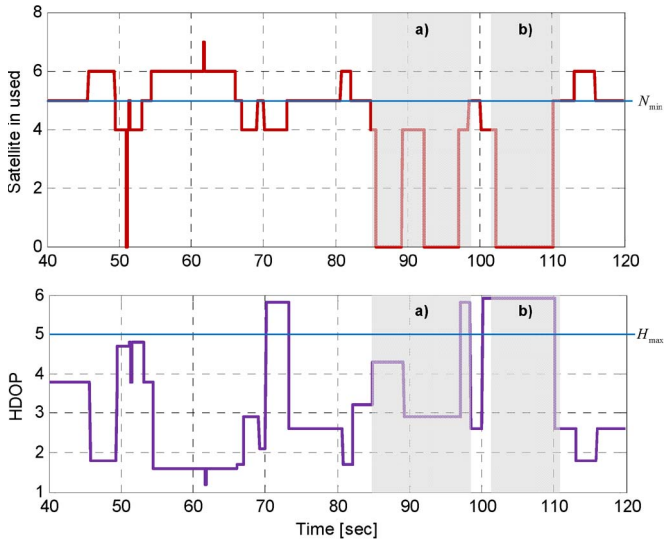

Fig. 16. Number of satellites used and the HDOP for the GPS receiver. The thresholds $N_{\min}$ and $H_{\max}$ for the rule-based update algorithm are both five.

We verified this positioning algorithm through simulations and experiments. The purpose of the simulation was an analysis of the relationship between the tire slip angle and each vehicle model. While the estimation performance of the kinematic vehicle model EKF was better than that of the dynamic vehicle model EKF for the low tire slip condition, the dynamic vehicle model EKF had better estimation performance for the large tire slip condition. The experiments were performed in various driving environments, such as parking lots, intersections, curved roads, and in a region with bad GPS signal that was surrounded by tall buildings. The experimental results showed that the estimates of the developed algorithm were accurate and reliable under the various driving conditions.

Due to the limitations of the two degrees-of-freedom bicycle model, the estimation of vehicle position in a very steep sloped driving environment and a large longitudinal tire slip condition was prohibited. In future work, the authors plan to extend the positioning algorithm to consider more dynamic states of road slope and longitudinal tire slip. The limitation might be compensated for by applying the longitudinal acceleration data to the positioning algorithm. The integration of the accelerometer and the wheel speed sensor in the positioning algorithm will improve the estimation of vehicle speed, which is very important for vehicle positioning [47].

REFERENCES

[1] S. Sukkarieh, E. M. Nebot, and H. F. Durrant-Whyte, "A high integrity IMU/GPS navigation loop for autonomous land vehicle applications," *IEEE Trans. Robot. Autom.*, vol. 15, no. 3, pp. 572–578, Jun. 1999.

[2] G. Dissanayake, S. Sukkarieh, E. Nebot, and H. Durrant-Whyte, "The aiding of a low-cost strapdown inertial measurement unit using vehicle model constraints for land vehicle applications," *IEEE Trans. Robot. Autom.*, vol. 17, no. 5, pp. 731–747, Oct. 2001.

[3] S. Panzieri, F. Pascucci, and G. Ulivi, "An outdoor navigation system using GPS and inertial platform," *IEEE/ASME Trans. Mechatronics*, vol. 7, no. 2, pp. 134–142, Jun. 2002.

[4] H. Qi and J. B. Moore, "Direct Kalman filtering approach for GPS/INS integration," *IEEE Trans. Aerosp. Electron. Syst.*, vol. 38, no. 2, pp. 687–693, Apr. 2002.

[5] D. Huang and H. Leung, "EM-IMM based land-vehicle navigation with GPS/INS," in *Proc. IEEE ITSC*, Washington, DC, 2004, pp. 624–629.

[6] F. Caron, E. Duflos, D. Pomorski, and P. Vanheeghe, "GPS/IMU data fusion using multisensor Kalman filtering: Introduction of contextual aspects," *Inf. Fusion*, vol. 7, no. 2, pp. 221–230, Jun. 2006.

[7] S. Godha and M. E. Cannon, "GPS/MEMS INS integrated system for navigation in urban areas," *GPS Solutions*, vol. 11, no. 3, pp. 193–203, 2007.

[8] R. Toledo-Moreo, M. A. Zamora-Izquierdo, B. Ubeda-Minarro, and A. F. Gomez-Skarmeta, "High-integrity IMM-EKF-based road vehicle navigation with low-cost GPS/SBAS/INS," *IEEE Trans. Intell. Transp. Syst.*, vol. 8, no. 3, pp. 491–511, Sep. 2007.

[9] R. Toledo-Moreo and M. A. Zamora-Izquierdo, "IMM-based lane-change prediction in highways with low-cost GPS/INS," *IEEE Trans. Intell. Transp. Syst.*, vol. 10, no. 1, pp. 180–185, Mar. 2009.

[10] J. Huang and H. S. Tan, "A low-order DGPS-based vehicle positioning system under urban environment," *IEEE/ASME Trans. Mechatronics*, vol. 11, no. 5, pp. 567–575, Oct. 2006.
[11] S. Rezaei and R. Sengupta, "Kalman filter-based integration of DGPS and vehicle sensors for localization," *IEEE Trans. Control Syst. Technol.*, vol. 15, no. 6, pp. 1080–1088, Nov. 2007.
[12] G. Fiengo, D. Di Domenico, and L. Glielmo, "A hybrid procedure strategy for vehicle localization system: Design and prototyping," *Control Eng. Pract.*, vol. 17, no. 1, pp. 14–25, Jan. 2009.
[13] H. Weinberg, "MEMS inertial sensor use growing for automotive applications," *Channel E Mag. Electron.*, 2005. [Online]. Available: http://www.channel-e.biz/design/articles/inertialsensor.html.
[14] R. Dixon and J. Bouchaud, "Prospects for MEMS in the automotive industry," *Sens. Transducers J.*, vol. 86, no. 12, pp. 1778–1784, Dec. 2007.
[15] T. K. Xia, M. Yang, and R. Q. Yang, "Vision based global localization for intelligent vehicles," in *Proc. IEEE Intell. Vehicles Symp.*, Tokyo, Japan, 2006, pp. 571–576.
[16] S. X. Wu and M. Yang, "Landmark pair based localization for intelligent vehicles using laser radar," in *Proc. IEEE Intell. Vehicles Symp.*, Istanbul, Turkey, 2007, pp. 209–214.
[17] T. Weiss, N. Kaempchen, and K. Dietmayer, "Precise ego-localization in urban areas using laserscanner and high accuracy feature maps," in *Proc. IEEE Intell. Vehicles Symp.*, Las Vegas, NV, 2005, pp. 284–289.
[18] H. Uchiyama, D. Deguchi, T. Takahashi, I. Ide, and H. Murase, "Ego-localization using streetscape image sequences from in-vehicle cameras," in *Proc. IEEE Intell. Vehicles Symp.*, Xi'an, China, 2009, pp. 185–190.
[19] N. Mattern, R. Schubert, and G. Wanielik, "High-accurate vehicle localization using digital maps and coherency images," in *Proc. IEEE Intell. Vehicles Symp.*, La Jolla, CA, 2010, pp. 462–469.
[20] R. G. García-García, M. A. Sotelo, I. Parra, D. Fernández, and M. Gavilán, "3D visual odometry for GPS navigation assistance," in *Proc. IEEE Intell. Vehicles Symp.*, Istanbul, Turkey, 2007, pp. 444–449.
[21] F. Chausse, J. Laneurit, and R. Chapuis, "Vehicle localization on a digital map using particles filtering," in *Proc. IEEE Intell. Vehicles Symp.*, Las Vegas, NV, 2005, pp. 243–248.
[22] D. Bétaille and R. Toledo-Moreo, "Creating enhanced maps for lane-level vehicle navigation," *IEEE Trans. Intell. Transp. Syst.*, vol. 11, no. 4, pp. 786–798, Dec. 2010.
[23] R. Toledo-Moreo, D. Betaille, and F. Peyret, "Lane-level integrity provision for navigation and map matching with GNSS, dead reckoning, and enhanced maps," *IEEE Trans. Intell. Transp. Syst.*, vol. 11, no. 1, pp. 100–112, Mar. 2010.
[24] N. Suganuma and T. Uozumi, "Precise position estimation of autonomous vehicle based on map-matching," in *Proc. IEEE Intell. Vehicles Symp. (IV)*, 2011, pp. 296–301.
[25] V. Popescu, M. Bace, and S. Nedevschi, "Lane identification and ego-vehicle accurate global positioning in intersections," in *Proc. IEEE Intell. Vehicles Symp. (IV)*, 2011, pp. 870–875.
[26] A. U. Peker, O. Tosun, and T. Acarman, "Particle filter vehicle localization and map-matching using map topology," in *Proc. IEEE Intell. Vehicles Symp. (IV)*, 2011, pp. 248–253.
[27] H. Badino, D. Huber, and T. Kanade, "Visual topometric localization," in *Proc. IEEE Intell. Vehicles Symp. (IV)*, 2011, pp. 794–799.
[28] I. Skog and P. Handel, "In-car positioning and navigation technologies: A survey," *IEEE Trans. Intell. Transp. Syst.*, vol. 10, no. 1, pp. 4–21, Mar. 2009.
[29] Y. Cui and S. S. Ge, "Autonomous vehicle positioning with GPS in urban canyon environments," *IEEE Trans. Robot. Autom.*, vol. 19, no. 1, pp. 15–25, Feb. 2003.
[30] N. Cui, L. Hong, and J. R. Layne, "A comparison of nonlinear filtering approaches with an application to ground target tracking," *Signal Process.*, vol. 85, no. 8, pp. 1469–1492, Aug. 2005.
[31] S. J. Julier and H. F. Durrant-Whyte, "On the role of process models in autonomous land vehicle navigation systems," *IEEE Trans. Robot. Autom.*, vol. 19, no. 1, pp. 1–14, Feb. 2003.
[32] Y. Bar-Shalom, X. Li, and T. Kirubarajan, *Estimation With Applications to Tracking and Navigation*. New York: Wiley-Interscience, 2001.
[33] H. Tsunashima, M. Murakami, and J. Miyata, "Vehicle and road state estimation using interacting multiple model approach," *Vehicle Syst. Dyn.*, vol. 44, pp. 750–758, 2006.
[34] H. A. P. Blom and Y. Bar-Shalom, "Interacting multiple model algorithm for systems with Markovian switching coefficients," *IEEE Trans. Autom. Control*, vol. 33, no. 8, pp. 780–783, Aug. 1988.
[35] C. Barrios, H. Himberg, Y. Motai, and A. Sadek, "Multiple model framework of adaptive extended Kalman filtering for predicting vehicle location," in *Proc. IEEE ITSC*, Toronto, ON, Canada, 2006, pp. 1053–1059.
[36] A. N. Ndjeng, S. Glaser, and D. Gruyer, "A multiple model localization system for outdoor vehicles," in *Proc. IEEE Intell. Vehicles Symp.*, Istanbul, Turkey, 2007, pp. 1050–1055.
[37] M. Dawood, C. Cappelle, M. E. El Najjar, M. Khalil, and D. Pomorski, "Vehicle geo-localization based on IMM-UKF data fusion using a GPS receiver, a video camera and a 3D city model," in *Proc. IEEE Intell. Vehicles Symp. (IV)*, 2011, pp. 510–515.
[38] X. R. Li and Y. Bar-Shalom, "Multiple-model estimation with variable structure," *IEEE Trans. Autom. Control*, vol. 41, no. 4, pp. 478–493, Apr. 1996.
[39] W. Travis and D. M. Bevly, "Navigation errors introduced by ground vehicle dynamics," in *Proc. 18th Int. Tech. Meeting Satellite Div. Inst. Navigat., ION GNSS*, Long Beach, CA, 2005, pp. 302–310.
[40] R. Rajamani, *Vehicle Dynamics and Control*. New York: Springer-Verlag, 2006.
[41] R. Pepy, A. Lambert, and H. Mounier, "Path planning using a dynamic vehicle model," in *Proc. 2nd ICTTA*, 2006, pp. 781–786.
[42] S. Taheri, "An investigation and design of slip control braking systems integrated with four wheel steering," Ph.D. dissertation, Clemson Univ., Clemson, SC, 1990.
[43] S. S. Blackman and R. Popoli, *Design and Analysis of Modern Tracking Systems*. Noorwood, MA: Artech House, 1999.
[44] G. Welch and G. Bishop, *An Introduction to the Kalman Filter*. Chapel Hill, NC: Univ. North Carolina Press, 1995.
[45] D. M. Bevly, J. C. Gerdes, C. Wilson, and G. Zhang, "Use of GPS based velocity measurements for improved vehicle state estimation," in *Proc. Amer. Control Conf.*, Chicago, IL, 2000, pp. 2538–2542.
[46] Y. Bar-Shalom, *Tracking and Data Association*. San Diego, CA: Academic, 1987.
[47] M. Tanelli, L. Piroddi, and S. M. Savaresi, "Real-time identification of tire-road friction conditions," *IET Control Theory Appl.*, vol. 3, no. 7, pp. 891–906, Jul. 2009.

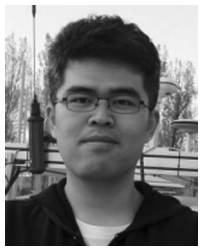

Kichun Jo (S'10) received the B.S. degree in mechanical engineering in 2008 from Hanyang University, Seoul, Korea, where he is currently working toward the Ph.D. degree with the Automotive Control and Electronics Laboratory.

His main fields of interest are information fusion theories and applications for vehicle localization and tracking, controller design, and system integration of intelligent vehicles. He has also worked on model-based embedded software development for automotive control systems.

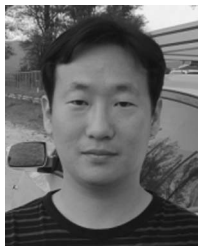

Keounyup Chu (S'10) received the B.S. degree in mechanical engineering and the M.S. and Ph.D. degrees in automotive engineering from Hanyang University, Seoul, Korea, in 2004, 2006, and 2011, respectively.

He is currently with the Automotive Control and Electronics Laboratory, Hanyang University. His research activities include the design of intelligent vehicles, real-time systems, distributed control systems, and in-vehicle networks. His current research interests are in motion planning and collision mitigation. He has also worked on the development of an autonomous vehicle.

Myoungho Sunwoo (M'81) received the B.S. degree in electrical engineering from Hanyang University, Seoul, Korea, in 1979, the M.S. degree in electrical engineering from the University of Texas at Austin in 1983, and the Ph.D. degree in system engineering from Oakland University, Rochester, MI, in 1990.

He joined General Motors Research (GMR) Laboratories, Warren, MI, in 1985 and has been working in the area of automotive electronics and control for 26 years. During his nine-year tenure at GMR, he worked on the design and development of various electronic control systems for power train and chassis. Since 1993, he has led research activities as a Professor with the Department of Automotive Engineering, Hanyang University: one of the largest engineering schools in Korea. His work has focused on automotive electronics and control such as modeling and control of internal combustion engines, design of automotive distributed real-time control systems, intelligent autonomous vehicles, and automotive education programs. During his professional career, he has published 55 international journal papers and 68 international conference papers and has held 19 patents. In addition, he successfully accomplished more than 50 research projects with the Korean government and automotive companies such as Hyundai, Kia, Mando, Hyundai MOBIS, Freescale, and many others. He has continuously consulted for the Korean government and the automotive industry.

Dr. Sunwoo currently serves as the Chairman of the steering committee for the Green Car Strategy Forum of the Ministry of the Knowledge Economy and is also an Academician of the National Academy of Engineering of Korea. His laboratory, i.e., ACE Lab, has been selected as a National Research Laboratory by the Korean government because of its outstanding research accomplishments. His autonomous vehicle named "A1" won the first National Autonomous Vehicle Competition organized by Hyundai Motor Company hosted in Korea in November 2010. In recognition of his distinguished achievements, he has received notable awards, such as the Grand Award of Academic-Industrial Cooperation from the Korean Academic-Industrial Foundation, the Best Scientist/Engineer Award of the Month from the Korean Ministry of Science and Technology, and the Award for Technology Innovation from the Prime Minister of Korea.